Article

Visualization of Lung Inflammation to Pulmonary Fibrosis via Peroxynitrite Fluctuation

Zixuan Zhan, Rui Liu, Li Chai, Yongcheng Dai, and Yi Lv

Anal. Chem., **Just Accepted Manuscript** • DOI: 10.1021/acs.analchem.9b02971 • Publication Date (Web): 30 Jul 2019

Visualization of Lung Inflammation to Pulmonary Fibrosis via Peroxynitrite Fluctuation

Zixuan Zhan†, Rui Liu†, Li Chai, § Yongcheng Dai† and Yi Lv† ‡*

†Key Laboratory of Green Chemistry & Technology, Ministry of Education, College of Chemistry, Sichuan University, Chengdu, Sichuan 610064, China
‡Analytical & Testing Center, Sichuan University, Chengdu, Sichuan 610064, China
§Core Facility of West China Hospital, Sichuan University, Chengdu, Sichuan, 610041, China
E-mail: lvy@scu.edu.cn; Tel & Fax: +86 28 85412798

ABSTRACT: Idiopathic pulmonary fibrosis (IPF) is a chronic and progressive lung disease with short survival time. However, owing to the unknown etiology and the lack of sensitive and noninvasive methods, the diagnosis of IPF in early stage is still full of challenges. Since the levels of oxidative stress in mitochondria is relevant to pulmonary fibrosis, we herein present a simultaneous NIR-Ia window and ratiometic fluorescent probe **rTPONOO-1** with two-photon and mitochondria targeting abilities to explore the potential biological roles of peroxynitrite ($ONOO^-$) in different states of lung slices from healthy to lung inflammation and pulmonary fibrosis, and there is a good linear relationship between ratiometric fluorescence changes and the rate of pulmonary fibrosis from H&E and Masson staining. In addition, the therapeutic efficacy of aminoguanidine hemisulfate salt (AG) was also investigated. Thus, **rTPONOO-1** has great potential in quickly predicting the progression of pulmonary fibrosis in early stage and improving effective treatment.

Idiopathic pulmonary fibrosis (IPF) is one of the most frequent chronic and progressive fibrotic interstitial lung diseases with an average survival time of 3 years without transplant once diagnosed.[1-3] In recent years, a growing number of studies were trying to figure out the precise pathogenic mechanisms of idiopathic pulmonary fibrosis. However, the exact etiology is still unknown. Although, the approaches for diagnosing IPF have improved significantly, the misdiagnosed and managed inappropriately therapy occurs frequently. Thus, the early recognition and determination the process of lung inflammation to pulmonary fibrosis may be of significant importance for predicting disease progression and improving effective treatment.[4,5]

Up to now, great efforts have been made to develep noninvasive imaging techniques for IPF diagnosis and treatment monitoring,[6-8] including magnetic resonance imaging (MRI),[9] computed tomography (CT),[10] single-photon emission computed tomography (SPECT),[11,12] positron emission tomography (PET),[13-15] optical imaging (OI).[16] However, the low concentration of biomakers in early stage of IPF make it difficult to quantify the activity of fibrosis. Given the high sensitivity of fluorescent probe for markers detecting, the approaches for imaging targets have potential in monitoring dynamic changes of IPF from early stage.

It has been reported that chronic inflammation and oxidative stress play significant roles in modulating fibrogenic process.[17,18] In addition, the levels of ROS and $ONOO^-$ are illuminated in inverse proportion with pulmonary function in IPF and may predict disease severity.[19-21] Moreover, the oxidative stress in mitochondria is related to the development of lung fibrosis.[22] Nonetheless, the potential biological roles of $ONOO^-$ for the development of pulmonary fibrosis have not yet been fully understood. Thus, it is vitally necessary and important to develop an effective fluorescent probe to investigate the pathophysiological mechanism of $ONOO^-$ in mitochondria and explore its role in the process of lung inflammation to pulmonary fibrosis.

Recently, numbers of fluorescent probes for $ONOO^-$ imaging in living cells have been developed.[23-40] Compared with one-photon fluorescent probes for $ONOO^-$ detecting, two-photon fluorescent probe exhibit higher temporal spatial resolution, deeper imaging depth, less background fluorescence and photobleaching.[41-44] Furthermore, ratiometric fluorescent probes with two emission signals were known to effectively mitigate the substantial interferences, including instrumental parameters, probe microenvironment and concentration, photobleaching and so on.[45-54] Among them, Chang and co-workers developed an excellent fluorescence resonance energy transfer (FRET) based probe for $ONOO^-$ imaging which possesses both two-photon and ratiometric properties.[55] In general, the distance of FRET-based probes between energy donors and acceptors need accurately regulate or the FRET efficiency would be seriously affected. Besides, ratiometric probes that emit light in the NIR-Ia window (700–900 nm) have aroused great interest in bioimaging.[56] To meet the demand for visualization the process of lung inflammation to pulmonary fibrosis via $ONOO^-$ fluctuation, we herein present a simultaneous NIR-Ia and ratiometric fluorescent

probe **rTPONOO-1** with two-photon and mitochondria targeting abilities for sensitive and selective detection $ONOO^-$ with fast response. And there is a good linear relationship between ratiometric fluorescence changes and the rate of pulmonary fibrosis from H&E and Masson staining. Moreover, we also investigate the remediation effect of AG for pulmonary fibrosis.

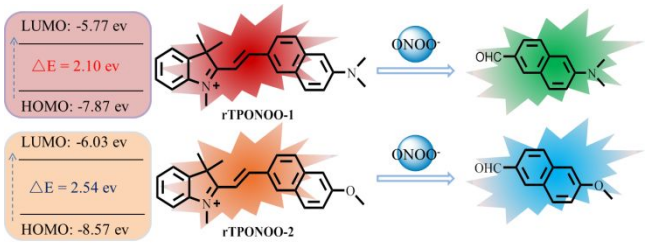

Figure 1. Energy levels of **rTPONOO-1** and **rTPONOO-2**.

EXPERIMENTAL SECTION

Chemicals and Instrumentations. All reagents were purchased from commercial suppliers and were used without purification. HRMS spectral data and MS spectral were recorded on a Bruker Daltonics Bio TOF mass spectrometer and a Finnigan LCQ^{DECA}, respectively. Photoluminescence spectra was recorded in Hitachi F-7000 fluorescence spectrophotometer. Cells and tissue imaging was performed with a Nikon Ni-E multiphoton laser scanning confocal microscope. BD FACSAria SORP was used to recorded flow cytometry data.

Synthesis of of 6-bromo-N,N-dimethylnaphthalen-2-amine (1). 40% Dimethylamine solution (6.4 mL, 50 mmol) was added to the mixture of compound 1 (2.22 g, 10 mmol) and $Na_2S_2O_5$ (3.8 g, 20 mmol) in H_2O (30 mL). The mixture was stirred in a steel-bomb reactor at 140 °C for 48 h. After filtering the solid product and washing with water till the filtrate was neutral, the product was purified in column chromatography using petroleum ether-DCM 3:1 (v/v) as the eluent to afford compound 2 (1.52 g, 61.0% yield). ^1H NMR (400 MHz, $CDCl_3$) δ (ppm): 7.83 (1H, s), 7.61 (1H, d, J = 9.2 Hz), 7.52 (1H, d, J = 8.8 Hz), 7.41 (1H, d, J = 8.8 Hz), 7.17 (1H, d, J = 8.4 Hz), 6.88 (1H, s), 3.05 (6H, s). ^{13}C NMR (400 MHz, $CDCl_3$) δ (ppm): 133.36, 129.34, 127.82, 117.04, 40.76. HR-ESI-MS m/z: calcd 250.0231, found 250.0203 $[M+H]^+$.

Synthesis of 6-(dimethylamino)-2-naphthaldehyde (2). A solution of n-BuLi (4.9 mL, 2.5M in hexane, 12 mmol) was added to a three-necked flask containing compound 2 (2.5 g, 10 mmol) in 10 mL anhydrous THF at -78 °C under N_2 atmosphere. The reaction was stirred at -78 °C for 0.75 h and then DMF (1.6 mL, 20 mmol) was added. Then, the reaction was quenched with saturated NH_4Cl after stirring at room temperature for 2 h. The crude product was extracted with ethyl acetate (EtOAc), and then using petroleum ether-EtOAc 6:1 (v/v) as the eluent to purify the product in column chromatography. (1.56 g, 78% yield). ^1H NMR (400 MHz, $CDCl_3$) δ (ppm): 10.01 (1H, s), 8.15 (1H, s), 7.83 (2H, d, J = 8.8 Hz), 7.66 (1H, d, J = 8.4 Hz), 7.19 (1H, dd, J_1 = 1.2 Hz, J_2 = 8.8 Hz), 6.91 (1H, s), 3.13 (6H, s). ^{13}C NMR (400 MHz, $CDCl_3$) δ (ppm): 191.81, 138.55, 134.81, 130.76, 126.84, 123.49, 116.23, 40.49. HR-ESI-MS m/z: calcd 200.1075, found 200.1062 $[M+H]^+$.

Synthesis of rTPONOO-1 (3). Compound 3 (498 mg, 2.5 mmol) and compound 4 (790 mg 2.5 mmol) were dissolved in absolute (25 mL). Subsequently, 1 mL piperidine was added to the flask. The reaction was refluxed for 12 h. Then, the reaction was cooled to room temperature and methanol was removed under reduced pressure. The product was purified on silica-gel column using DCM-Methanol 20:1 (v/v) as the eluent to yield **rTPONOO-1** (364 mg, 41% yield) ^1H NMR (400 MHz, $CDCl_3$) δ (ppm): 8.54 (1H, s), 8.25 (1H, d, J = 15.6 Hz), 8.03 (1H, d, J = 8.8 Hz), 7.94 (1H, d, J = 8.8 Hz), 7.69 (1H, d, J = 15.6 Hz), 7.63 (1H, d, J = 8.4 Hz), 7.51 (4H, s), 7.08 (1H, dd, J_1 = 1.6 Hz, J_2 = 8.8 Hz), 6.78 (1H, s), 4.32 (3H, s), 3.13 (6H, s), 1.82 (6H, s). ^{13}C NMR (400 MHz, $CDCl_3$) δ (ppm): 180.52, 155.61, 151.33, 142.36, 141.60, 138.84, 136.58, 132.19, 129.42, 128.79, 127.50, 127.39, 125.94, 125.65, 122.38, 116.03, 113.94, 108.87, 105.45, 51.65, 40.33, 35.81, 27.29. HR-ESI-MS m/z: calcd 355.2169, found 355.2148 $[M+H]^+$.

Synthesis of rTPONOO-2 (4). Compound 5 (0.92 g, 5 mmol) and compound 4 (1.58 g 5 mmol) were dissolved in absolute methanol (50 mL). Subsequently, 1 ml piperidine was added to the flask. The reaction was refluxed for 12 h. **rTPONOO-2** (1.32 g, 56.3% yield) was obtained as the process of **rTPONOO-1** ^1H NMR (400 MHz, $CDCl_3$) δ (ppm): 8.69 (1H, s), 8.34 (1H, d, J = 16.4 Hz), 8.21 (1H, d, J = 8.8 Hz), 8.01 (1H, d, J = 9.2 Hz), 7.89 (1H, d, J = 16 Hz), 7.80 (1H, d, J = 8.4 Hz), 7.53 (4H, s), 7.15 (1H, dd, J_1 = 1.6 Hz, J_2 = 8.8 Hz), 7.09 (1H, d, J = 2.0 Hz), 4.44 (3H, s), 3.93 (3H, s), 1.85 (6H, s). ^{13}C NMR (400 MHz, $CDCl_3$) δ (ppm): 181.80, 160.77, 155.30, 142.72, 141.41, 138.06, 135.07, 131.84, 129.60, 129.59, 129.31, 128.50, 128.25, 126.10, 122.48, 120.00, 114.60, 111.64, 106.17, 55.58, 52.25, 36.95, 27.04. HR-ESI-MS m/z: calcd 342.1852, found 342.1816 $[M+H]^+$.

Two-Photon Tissue Imaging. Before animal imaging, C57BL/6 mouse were starved for 12 h to rule out the possible of food fluorescence interference at the emission band of **rTPONOO-1**. Tissue slices of lungs were harvested and embedded in tissue-freezing medium, frozen and consecutively cryo-sectioned into 10 μm. The slices were cultured with 20 μM **rTPONOO-1** for 1 h and then incubated with 200 μM $ONOO^-$ for another 1 h. Before imaging experiments, the slices were washed three times with PBS solution.

Bleomycin-Induced Pulmonary Injury to Pulmonary Fibrosis and Remediation Effect of AG. For bleomycin-induced pulmonary injury to pulmonary fibrosis, after 1 week acclimation, the animals were randomly allocated to 12 groups (5 animal in each). All the C57BL/6 mice used in this study were 6 to 8 weeks old. Before intratracheal delivery bleomycin or saline, mice were anesthetized intraperitoneally with 10% chloralic hydras (3.5 mg/kg). Then, mice in group (1)、(3)、(5)、(7)、(9) received intratracheal instillation of a single dose of sterile normal saline (0.1 mL)、bleomycin (1 mg/Kg, 0.1 mL)、bleomycin (2 mg/Kg, 0.1 mL)、bleomycin (3 mg/Kg, 0.1 mL)、bleomycin (3 mg/Kg, 0.1 mL), followed by daily ip injection of aminoguanidine hemisulfate salt (20 mg/kg/d),

respectively. Mice in group (2) 、(4) 、(6) 、(8) 、(10) received intratracheal instillation of a single dose of sterile normal saline (0.1 mL)、bleomycin (1 mg/Kg, 0.1 mL)、bleomycin (2 mg/Kg, 0.1 mL)、bleomycin (3 mg/Kg, 0.1 mL)、bleomycin (3 mg/Kg, 0.1 mL), followed by daily ip injection of aminoguanidine hemisulfate salt (20 mg/kg/d), respectively. And then **rTPONOO-1** (50 μM, 0.1 mL) was intramuscularly injected through tail vein for 30 min. All mice were sacrificed on day 14 after injection of **rTPONOO-1** for 30 min. Finally, animal necropsies were carried out, lung tissues of group (1)、(3)、(5)、(7)、(9) were collected for H&E and Masson staining, lung tissues of group (2) 、(4) 、(6) 、(8) 、(10) were collected for imaging.

RESULTS AND DISCUSSION

Design and Synthesis of Probe for ONOO⁻. The design and synthesis of probes were shown in Scheme S1, **rTPONOO-1** and **rTPONOO-2** were conveniently sythesized by direct condensation of a typical two-photon fluorophore acedan and an indolium derivative. The structure of **rTPONOO-1** and **rTPONOO-2** were comfirmed by ^{1}H NMR, ^{13}C NMR and HRMS in Figure S1. Comparing to the yellow emission of **rTPONOO-2**, **rTPONOO-1** exhibits NIR-1a emission due to the stronger "push−pull" structure. The result was consistent with the calculation that the smaller energy band gap could make a larger emission red shift (Figure 1 and Figure S2). What's more, the positive charge of **rTPONOO-1** may possess high specificity for mitochondria targeting. Thus, we expected that the NIR-1a emission **rTPONOO-1** could accumulate in mitochondria and the C=C bond would be oxidized and cleaved by ONOO⁻ to release the green emission two-photon fluorophore, leading to a ratiometric response to ONOO⁻.

Ratiometric Response towards ONOO⁻. We first evaluated the optical properties of **rTPONOO-1** and **rTPONOO-2** before and after addition of ONOO⁻ in PBS buffer solution containing 1% DMF (50 mM, pH = 7.4). As indicated in Figure S3, the absorption spectrum and color of **rTPONOO-1** and **rTPONOO-2** have remarkable changes upon addition of ONOO⁻. Then, a series of reaction conditions of **rTPONOO-1** and **rTPONOO-2** toward ONOO⁻ were conducted. As shown in Figure S4, the ratio fluorescence intensity of **rTPONOO-1** and **rTPONOO-2** almost have no change within the pH range of 6 – 8. After addition of ONOO⁻, the I_{535}/I_{718} and I_{470}/I_{575} ratio increase with the increase of pH. Considering the basic pH (pH ≈ 8) in mitochondria,[57] the probes have potential in detecting ONOO⁻ in mitochondria of living cells. In addition, the time-dependent ratio fluorescence of **rTPONOO-1** and **rTPONOO-2** in the presence of 0, 5 equiv, 10 equiv of ONOO⁻ was recorded. As shown in Figure S5, the probes are very stable with no obvious ratio change, and the reaction between probes and ONOO⁻ was fast. Owning to the larger emission shift, greater ratio change of **rTPONOO-1** toward ONOO⁻, **rTPONOO-1** is more suitable for tracking ONOO⁻ in living systems. Thus, **rTPONOO-1** was chosen for subsequent experiments.

Subsequently, to evaluate the specificity of **rTPONOO-1** toward ONOO⁻, various reactive oxygen species (ROS) and other biologically relevant analytes were investigated

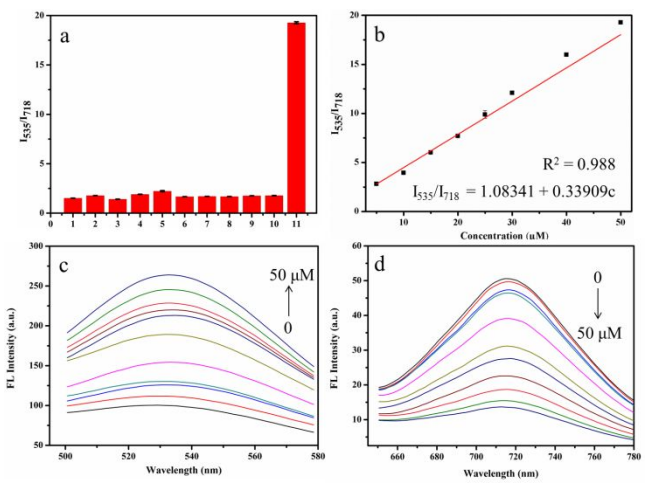

Figure 2. (a) The fluorescence ratio (I_{535}/I_{718}) of **rTPONOO-1** (5 μM) in the presence of ONOO⁻ (50 μM) and biologically relevant analytes (100 μM) [1, **rTPONOO-1**; 2, GSH; 3, Cys; 4, H_2O_2; 5, HOCl; 6, TBHP; 7, NO; 8, •OH; 9, $•O_2^-$; 10, O_2^1; 11, ONOO⁻] in PBS buffer solution containing 1% DMF (50 mM, pH = 7.4). (λ_{ex} = 375 nm and λ_{ex} = 525 nm). (b) The linear relationship between fluorescence ratio (I_{535}/I_{718}) of **rTPONOO-1** (5 μM) and different concentrations of ONOO⁻ (5 – 50 μM) (c) The emission spectrum of **rTPONOO-1** after treating with different concentrations of ONOO⁻ (0 – 50 μM) (λ_{ex} = 375 nm). (d) The emission spectrum of **rTPONOO-1** after treating with different concentrations of ONOO⁻ (0 – 50 μM) (λ_{ex} = 525 nm).

(Figure 2a and Figure S6). To our delight, even highly reactive oxygen radicals, including hypochlorous acid (HOCl), tert-butyl hydroperoxide (TBHP), superoxide ($•O_2^-$) and hydroxyl radical (•OH), almost have no influence on I_{535}/I_{718} ratio enhancement. In addition, there are also no ratio increment with other biologically relevant analytes. Only ONOO⁻ can lead to remarkable ratiometric fluorescence change, which indicated the highly selective of **rTPONOO-1** toward ONOO⁻. To confirm the sensing mechanism of **rTPONOO-1** toward ONOO⁻, ESI-MS analysis and NMR titration were conducted (Figure S7 and Figure S8). Furthermore, the fluorescence emission spectrum of **rTPONOO-1** toward different concentrations of ONOO⁻ was examined. As shown in Figure 2c and Figure 2d, the emission spectrum of **rTPONOO-1** at 718 nm decreased and 535 nm increased, respectively. Moreover, there is a good linear relationship between ratio fluorescence intensities (I_{535}/I_{718}) of **rTPONOO-1** and ONOO⁻ ranging from 5 – 50 μM. The detection limit was 85 nM, indicating the high sensitivity of **rTPONOO-1** toward ONOO⁻ (Figure 2b and Figure S9).

Mitochondria Targeting Ability of rTPONOO-1. Owning to the encouraging results above, the feasibility of **rTPONOO-1** for living cells imaging was evaluated. We first examined the cytotoxicity of **rTPONOO-1** with A549 and RAW 264.7. The result in Figure S10 indicated that **rTPONOO-1** has low cytotoxicity. It is known that ONOO⁻ is mainly produced in mitochondria and lipophilic cations have good permeability for mitochondria targeting.

Thus, a colocalization experiment was performed by co-staining A549 cells or RAW 264.7 cells with **rTPONOO-1** and a well-known commercial mitochondrial staining dye, Mito-tracker Green. As shown in Figure 3, the cells loaded with Mito-tracker Green and **rTPONOO-1** were well merged with a high Pearson's colocalization coefficient. In addition, the intensity profiles with yellow line across cells in the linear regions of interest (ROIs) altered in close synchrony. These results demonstrated that **rTPONOO-1** is capable of real time tracking $ONOO^-$ in mitochondria.

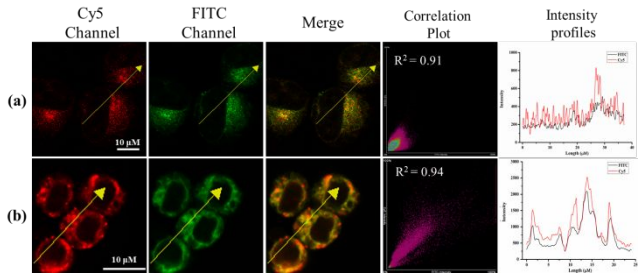

Figure 3. Intracellular localization of **rTPONOO-1** in (a) A549 cells (b) RAW 264.7 cells. Images of cells were pre-treated with **rTPONOO-1** (10 μM) for 30 min and then Mito-Tracker Green (500 nM) for another 30 min. Cy5 channel for **rTPONOO-1**: λ_{ex} = 488 nm; FITC channel for Mito-Tracker Green: λ_{ex} = 488 nm.

Ratiometric and Two-photon Visualizing Exogenous and Endogenous $ONOO^-$ in Living Cells. Subsequently, the potential ratiometric ability of **rTPONOO-1** for detecting and imaging $ONOO^-$ in living cells was evaluated. As indicated in Figure 4, the cells treated with **rTPONOO-1** displayed remarkable red fluorescence and weak green fluorescence. However, with the addition of different concentrations of SIN-1 ($ONOO^-$ donor), the fluorescence in green channel was greatly enhanced while a dramatic drop of fluorescence in red channel was observed. Thus, an obvious ratiometric fluorescence response (red/green) to $ONOO^-$ was established. Based on the promising result on ratiometric imaging $ONOO^-$ in A549 cells, we decided to verify the ratiometric response in flow cytometry. As expected, the result was consistent with the imaging response (Figure S11). Additionally, the feasibility of **rTPONOO-1** for imaging $ONOO^-$ with two-photon confocal fluorescence microscopy (TPM) was examined (Figure 4). The cells labeled with **rTPONOO-1** exhibited weak fluorescence in FITC channel under the excitation at 800 nm. To our delight, the cells incubated with **rTPONOO-1** and different concentrations of SIN-1 displayed remarkable fluorescence. These results indicated that **rTPONOO-1** have capacity to imaging exogenous ONOO- with ratiometric and two-photon response.

It has been reported that endogenous $ONOO^-$ can be produced in RAW 264.7 cells by stimulating of lipopolysaccharide(LPS) and interferon-gamma (IFN-γ). To examine whether **rTPONOO-1** can be applied to detect exogenous and endogenous $ONOO^-$ in living cells. RAW 264.7 cells were pre-treated with different concentrations of SIN-1 or stimulus, then incubated with **rTPONOO-1** for another 30 min. As illustrated in Figure 5, the cells treated with stimulus or SIN-1 showed remarkable ratiometric response, respectively. While cells loaded with N-acetylcysteine (NAC), a powerful ROS scavenger, displayed barely no fluorescence change in both two channels. Additionally, we

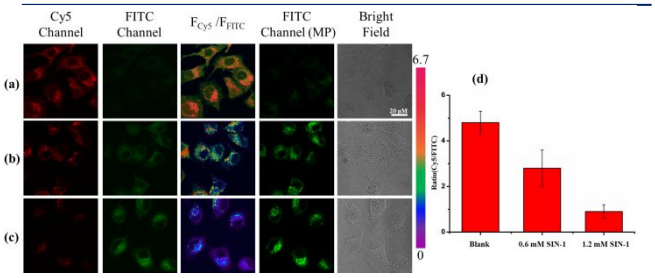

Figure 4. Imaging of $ONOO^-$ in A549 cells treated with (a) **rTPONOO-1** (10 μM) for 30 min; (b) **rTPONOO-1** (10 μM) for 30 min and then 0.6 mM SIN-1 for another 30 min; (c) **rTPONOO-1** (10 μM) for 30 min and then 1.2 mM SIN-1 for another 30 min; (d) Average intensity ratios from (a) - (c). Cy5 channel: λ_{ex} = 488 nm; FITC channel: λ_{ex} = 405 nm; FITC channel (MP): λ_{ex} = 800 nm.

also detect exogenous and endogenous $ONOO^-$ in flow cytometry (Figure S12). Not surprisingly, the ratiometric response was in accordance with the imaging result. Moreover, **rTPONOO-1** was also successfully applied to image endogenous $ONOO^-$ by TPM. These results implied that **rTPONOO-1** is available to detect and visualize endogenous $ONOO^-$ generation in RAW 264.7 cells.

Bleomycin-Induced Pulmonary Injury to Pulmonary Fibrosis and the Remediation Effect of AG. Inspired by the ratiometric and two-photon performance of **rTPONOO-1** for tracking both endogenous and exogenous $ONOO^-$ in living cells, we further explored whether **rTPONOO-1** can be used for tissue imaging. The experiment frozen lung slices were classified into two groups. The slices in the first group were treated with **rTPONOO-1** (20 μM) for 1 h while in the second group, the slices were treated with 20 μM **rTPONOO-1** for 1 h and then incubated with 200 μM $ONOO^-$ for another 1 h. As shown in Figure S13, compare to the fluorescence performance in the first group, the fluorescence in Cy5 channel have a significant decrease and there is obvious fluorescence increase in the FITC channel, making a remarkable ratiometric signal change. In addition, two-photon imaging of $ONOO^-$ was also conducted. Moreover, the fluorescence at different depths in the two groups were recorded by using z-scan mode of the TPM (Figure S14). It is able to visualize green fluorescence only in 70 μm depth in the first group, meanwhile, the fluorescence intensities of second group at 110 μm depths of mouse lung tissue can be detected.

These results motivate us to further extend its application for tracking the process from healthy lung to pulmonaryfibrosis and the remediation effect of AG. Thus, C57BL/6 mice were divided into ten groups and different concentrations of bleomycin were used to induce lung inflammation and pulmonary fibrosis. To evaluate the extent of pulmonary fibrosis and the therapeutic efficacy ofAG, H&E and Masson staining were conducted (Figure6).

Comparing to the control group, the low dose bleomycin group showed inflammatory cell infiltration, widened

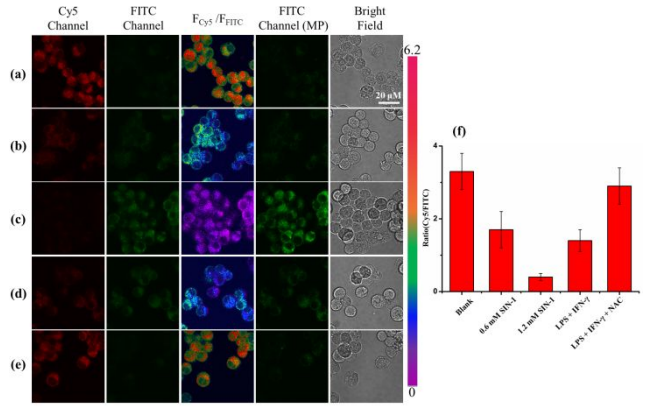

Figure 5. Imaging of exogenous and endogenous $ONOO^-$ in RAW 264.7 cells treated with (a) **rTPONOO-1** (10 μM) for 30 min; (b) 0.6 mM SIN-1 for 30 min and then **rTPONOO-1** (10 μM) for another 30 min; (c) 1.2 mM SIN-1 for 30 min and then **rTPONOO-1** (10 μM) for another 30 min; (d) LPS (1 μg/mL) and IFN-γ (50 ng/mL) for 12 h, and then **rTPONOO-1** (10 μM) for 30 min; (e) LPS (1 μg/mL), IFN-γ (50 ng/mL) and NAC (1 mM) for 12 h, then **rTPONOO-1** (10 μM) for 30 min; (f) Average intensity ratios from (a) - (e). Cy5 channel: λ_{ex} = 488 nm; FITC channel: λ_{ex} = 405 nm; FITC channel (MP): λ_{ex} = 800 nm.

alveolar spaces, and alveolar structure damage, while the high dose bleomycin group showed obvious pulmonary fibrosis. Moreover, AG could serve as an effective remediation reagent. We then explored the relationship between $ONOO^-$ levels and the degree of lung inflammation and pulmonary fibrosis. As shown in Figure. 7, the mice treated with bleomycin showed remarkable ratiometric fluorescence changes, indicating $ONOO^-$ could be a biomarker for pulmonary fibrosis. To our delight, there is a good linear relationship between the rate of pulmonary fibrosis from H&E and Masson staining and fluorescence ratios. These results demonstrated that **rTPONOO-1** can not only visualize pulmonary fibrosis via $ONOO^-$ fluctuation in early stage but also predict the effective treatment.

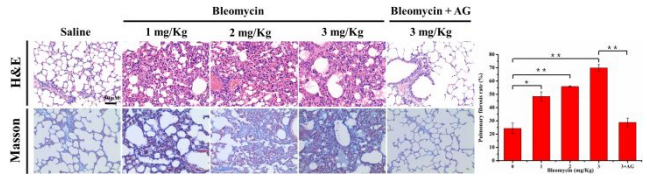

Figure 6. Bleomycin induced pulmonary fibrosis and remediation effect of AG. The values are the mean for n = 3, *p < 0.05, **p < 0.01.

CONCLUSIONS

In conclusion, we have developed a simultaneous NIR-Ia and ratiometic fluorescent probe **rTPONOO-1** with two-photon and mitochondria targeting abilities for visualization ratiometric fluorescence changes in different states of lung slices from healthy to lung Inflammation and pulmonary fibrosis via $ONOO^-$ fluctuation, and $ONOO^-$ could be a biomarker for pulmonary fibrosis. In addition,

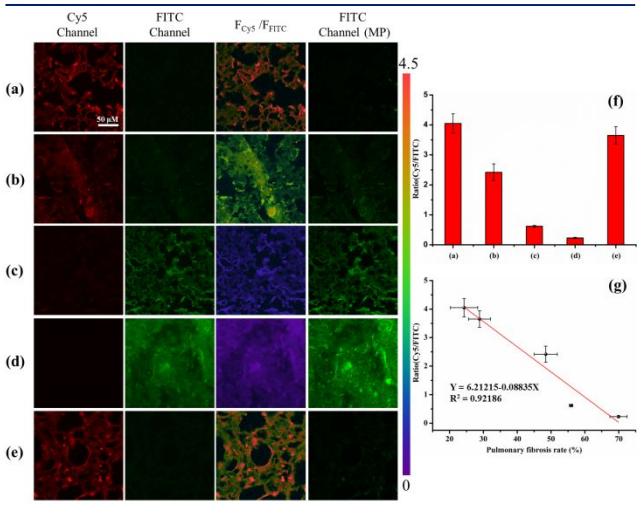

Figure 7. Imaging of $ONOO^-$ levels from healthy lung slices to lung inflammation and pulmonary fibrosis. Mice received intratracheal instillation of (a) sterile normal saline (0.1 mL); (b) bleomycin (1 mg/kg, 0.1 mL); (c) bleomycin (2 mg/kg, 0.1 mL); (d) bleomycin (3 mg/kg, 0.1 mL); (e) bleomycin (3 mg/kg, 0.1 mL) followed by daily ip injection of AG (20 mg/kg/d). And then **rTPONOO-1** (50 μM, 0.1 mL) for 30 min. (f) Average intensity ratios from (a) - (e); (g) The relationship between fluorescence ratios and the rate of pulmonary fibrosis. Cy5 channel: λ_{ex} = 488 nm; FITC channel: λ_{ex} = 405 nm; FITC channel (MP): λ_{ex} = 800 nm.

there is a good linear relationship between ratiometric fluorescence changes and the rate of pulmonary fibrosis from H&E and Masson staining. Moreover, AG could serve as an effective remediation reagent for pulmonary fibrosis. Thus, **rTPONOO-1** has great potential in predicting the progression of pulmonary fibrosis in early stage and improving effective treatment.

ASSOCIATED CONTENT

Supporting Information.
General experimental methods, spectral data, cells and tissue imaging.

AUTHOR INFORMATION

ORCID

Yi Lv: 0000-0002-7104-2414

Notes

The authors declare no competing financial interest.

ACKNOWLEDGMENT

We thank Prof. Pengchi Deng and Dr. Chenghui Li in Analytical & Testing Center of Sichuan University for technical assistance. This work was supported by the National Natural Science Foundation of China (Nos.

21575093 & 21874094) and the Recruitment Program of Global Experts of Sichuan Province (No. 903).

REFERENCES

(1) Sgalla, G.; Biffi, A.; Richeldi, L. Idiopathic pulmonary fibrosis: Diagnosis, epidemiology and natural history. *Respirology*. **2016**, *21*, 427-437.

(2) Lin, X.; Sine, P. J.; Xu, H.; Williams, M. A.; Larussa, L.; Georas, S. N.; Guo, J. Yin Yang 1 Is a Novel Regulator of Pulmonary Fibrosis. *Am. J. Respir. Crit. Care. Med.* **2011***, 183, 1689-1697.*

(3) Pullamsetti, S. S.; Savai, R.; Dumitrascu, R.; Dahal, B. K.; Wilhelm, J.; Konigshoff, M.; Zakrzewicz, D.; Ghofrani, H. A.; Weissmann, N.; Eickelberg, O.; Guenther, A.; Leiper, J.; Seeger, W.; Grimminger, F.; Schermuly, R. T. The Role of Dimethylarginine Dimethylaminohydrolase in Idiopathic Pulmonary Fibrosis. *Sci. Transl. Med*. **2011**, *3*, 87ra53.

(4) Albera, C.; Costabel, U.; Fagan, E. A.; Glassberg, M. K.; Gorina, E.; Lancaster, L.; Lederer, D. J.; Nathan, S. D.; Spirig, D.; Swigris, J. J. Efficacy of pirfenidone in patients with idiopathic pulmonary fibrosis with more preserved lung function. *Eur. Respir. J*. **2016**, *48*, 843-851.

(5) Kolb, M.; Richeldi, L.; Behr, J.; Maher, T. M.; Tang, W.; Stowasser, S.; Hallmann, C. Bois, R. M. D. Nintedanib in patients with idiopathic pulmonary fibrosis and preserved lung volume. *Thorax*. **2013**, *72*, 340-346.

(6) Baues, M.; Dasgupta, A.; Ehling, J.; Prakash, J.; Boor, P.; Tache, F.; Kiessling, F.; Lammers, T. Fibrosis imaging: Current concepts and future directions. *Advanced. Drug. Delivery. Reviews.* **2017**, *121*, 9-26.

(7) Montesi, S. B.; Désogère, P.; Fuchs, B. C.; Caravan, P. Molecular imaging of fibrosis: recent advances and future directions. *J. Clin. Invest*. **2019**, *129*, 24-33.

(8) Désogère, P.; Montesi, S. B.; Caravan, P. Molecular Probes for Imaging Fibrosis and Fibrogenesis. *Chem. - Eur. J*. **2019**, *25*, 1128-1141.

(9) Caravan, P.; Yang, Y.; Zachariah, R.; Schmitt, A.; Mino-Kenudson, M.; Chen, H. H.; Sosnovik, D. E.; Dai, G.; Fuchs, B. C.; Lanuti, M. Molecular Magnetic Resonance Imaging of Pulmonary Fibrosis in Mice. *Am. J. Respir. Cell Mol. Biol*. **2013**, *49*, 1120-1126.

(10) Noble, P. W.; Barkauskas, C. E.; Jiang, D. Pulmonary fibrosis: patterns and perpetrators. *J. Clin. Invest*. **2012**, *122*, 2756-2762.

(11) Muzard, J.; Sarda-Mantel, L.; Loyau, S.; Meulemans, A.; Louedec, L.; Bantsimba-Malanda, C.; Hervatin, F.; Marchal-Somme, J.; Michel, J. B.; Guludec, D. L.; Billiald, P.; Jandrot-Perrus, M. Non-Invasive Molecular Imaging of Fibrosis Using a Collagen-Targeted Peptidomimetic of the Platelet Collagen Receptor Glycoprotein VI. *PLoS One.* **2009**, *4*, e5585.

(12) Zheng, L.; Ding, X.; Liu, K.; Feng, S.; Tang, B.; Li, Q.; Huang, D.; Yang, S. Molecular imaging of fibrosis using a novel collagen‐binding peptide labelled with 99mTc on SPECT/CT. *Amino Acids* **2016**, *49*, 89-101.

(13) Désogère, P.; Tapias, L. F.; Hariri, L. P.; Rotile, N. J.; Rietz, T. A.; Probst, C. K.; Blasi, F.; Day, H.; Mino-Kenudson, M.; Weinreb, P.; Violette, S. M.; Fuchs, B. C.; Tager, A. M.; Lanuti, M.; Caravan, P. Type I collagen–targeted PET probe for pulmonary fibrosis detection and staging in preclinical models. *Sci. Transl. Med.* **2017**, *9*, eaaf4696.

(14) Désogère, P.; Tapias, L. F.; Rietz, T. A.; Rotile, N.; Blasi, F.; Day, H.; Elliott, J.; Fuchs, B. C.; Lanuti, M.; Caravan, P. Optimization of a Collagen-Targeted PET Probe for Molecular Imaging of Pulmonary Fibrosis. *J. Nucl. Med.* **2017**, *58*, 1991-1996.

(15) Wahsner, J.; Désogère, P.; Abston, E.; Graham-O'Regan, K. A.; Wang, J.; Rotile, N. J.; Schirmer, M. D.; Santos Ferreira, D. D.; Sui, J.; Fuchs, B. C.; Lanuti, M.; Caravan, P. ^{68}Ga-NODAGA-Indole: An Allysine-Reactive Positron Emission Tomography Probe for Molecular Imaging of Pulmonary Fibrogenesis. *J. Am. Chem. Soc.* **2019**, *141*, 5593-5596.

(16) Hwang, J.; Huang, Y.; Burwell, T. J.; Peterson, N. C.; Connor, J.; Weiss, S. J.; Yu, S. M.; Li, Y. In Situ Imaging of Tissue Remodeling with Collagen Hybridizing Peptides. *ACS Nano.* **2017**, *11*, 9825-9835.

(17) Teramoto, S.; Fukuchi, Y.; Uejima, Y.; Shu, C.; Orimo, H. Superoxide anion formation and glutathione metabolism of blood in patients with idiopathic pulmonary fibrosis. *Biochem. Mol. Med*. **1995**, *55*, 66-70.

(18) Kliment, C. R.; Oury, T. D. Oxidative stress, extracellular matrix targets, and idiopathic pulmonary fibrosis. *Free Radical Biology & Medicine.* **2010**, *49*, 707-717.

(19) Daniil, Z. D.; Papageorgiou, E.; Koutsokera, A.; Kostikas, K.; Kiropoulos, T.; Papaioannou, A. I.; Gourgoulianis, K. I. Serum levels of oxidative stress as a marker of disease severity in idiopathic pulmonary fibrosis. *Pulm. Pharmacol. Ther*. **2008**, *21*, 26-31.

(20) Saleh, D.; Barnes, P. J.; Giaid, A. Increased Production of the Potent Oxidant Peroxynitrite in the Lungs of Patients with Idiopathic Pulmonary Fibrosis. *Am. J. Respir. Crit. Care Med.* **1997**, *155*, 1763-1769.

(21) Chen, X.; Li, W.; Zhou, A.; Ai, J.; Huang, S. Role of endogenous peroxynitrite in pulmonary injury and fibrosis induced by bleomycin A_5 in rats. *Acta. Pharmacol. Sin.* **2003**, *14*, 697-702.

(22) Mora, A. L.; Rojas, M.; Pardo, A.; Selman, M. Emerging therapies for idiopathic pulmonary fibrosis, a progressive age-related disease. *Nat. Rev. Drug. Discov*. **2017**, *16*, 755-772.

(23) Yang, D.; Wang, H.; Sun, Z.; Chung, N.; Shen, J. A Highly Selective Fluorescent Probe for the Detection and Imaging of Peroxynitrite in Living Cells. *J. Am. Chem. Soc.* **2006**, *128*, 6004-6005.

(24) Yu, F.; Li, P.; Li, G.; Zhao, G.; Chu, T.; Han, K. A Near-IR Reversible Fluorescent Probe Modulated by Selenium for Monitoring Peroxynitrite and Imaging in Living Cells. *J. Am. Chem. Soc.* **2011**, *133*, 11030-11033.

(25) Zhang, Q.; Zhu, Z.; Zheng, Y.; Cheng, J.; Zhang, N.; Long, Y. T.; Zheng, J.; Qian, X.; Yang, Y. A Three-Channel Fluorescent Probe That Distinguishes Peroxynitrite from Hypochlorite. *J. Am. Chem. Soc.* **2012**, *134*, 18479-18482.

(26) Sun, X.; Xu, Q.; Kim, G.; Flower, S. E.; Lowe, J. P.; Yoon, J.; Fossey, J. S.; Qian, X.; Bull, S. D.; James, T. D. A water-soluble boronate-based fluorescent probe for the selective detection of peroxynitrite and imaging in living cells. *Chem. Sci.* **2014**, *5*, 3368.

(27) Hou, J.; Yang, J.; Li, K.; Liao, Y.; Yu, K.; Xie, Y.; Yu, X. A highly selective water-soluble optical probe for endogenous peroxynitrite. *Chem. Commun.* **2014**, *50*, 9947-9950.

(28) Peng, T.; Wong, N.; Chen, X.; Chan, Y.; Sun, Z.; Hu, J. J.; Shen, J.; El-Nezami, H.; Yang, D. Molecular Imaging of Peroxynitrite with HKGreen‐4 in Live Cells and Tissues. *J. Am. Chem. Soc.* **2014**, *136*, 11728-11734.

(29) Zhang, H.; Liu, J.; Sun, Y. Q.; Huo, Y.; Li, Y.; Liu, W.; Wu, X.; Zhu, N.; Shi, Y.; Guo, W. A mitochondria-targetable fluorescent probe for peroxynitrite: fast response and high selectivity. *Chem. Commun.* **2015**, *51*, 2721-2724.

(30) Li, X.; Tao, R. R.; Hong, L. J.; Cheng, J.; Jiang, Q.; Lu, Y. M.; Liao, M. H.; Ye, W. F.; Lu, N. N.; Han, F.; Hu, Y. Z.; Hu, Y. H. Visualizing Peroxynitrite Fluxes in Endothelial Cells Reveals the Dynamic Progression of Brain Vascular Injury. *J. Am. Chem. Soc.* **2015**, *137*, 12296-12303.

(31) Sedgwick, A. C.; Sun, X.; Kim, G.; Yoon, J.; Bull, S. D.; James, T. D. Boronate based fluorescence (ESIPT) probe for Peroxynitrite. *Chem. Commun.* **2016**, *52*, 12350-12352.

(32) Yudhistira, T.; Mulay, S. V.; Lee, K. J.; Kim, Y.; Park, H. S.; Churchill, D. G. Thiomaleimide Functionalization for Selective Biological Fluorescence Detection of Peroxynitrite as Tested in HeLa and RAW 264.7 Cells. *Chem. -Asian J*. **2017**, *12*, 1927-1934.

(33) Li, H.; Li, X.; Wu, X.; Shi, W.; Ma, H. Observation of the Generation of ONOO− in Mitochondria under Various Stimuli with a Sensitive Fluorescence Probe. *Anal Chem*. **2017**, *89*, 5519-5525.

(34) Cheng, D.; Xu, W.; Yuan, L.; Zhang, X. Investigation of Drug-Induced Hepatotoxicity and Its Remediation Pathway with Reaction-Based Fluorescent Probes. *Anal Chem*. **2017**, *89*, 7693-7700.

(35) Wu, D.; Ryu, J. C.; Chung, Y. W.; Lee, D.; Ryu, J. H.; Yoon, J. H.; Yoon, J. A Far-Red-Emitting Fluorescence Probe for Sensitive and Selective Detection of Peroxynitrite in Live Cells and Tissues. *Anal Chem*. **2017**, *89*, 10924-10931.

(36) Sedgwick, A. C.; Han, H.; Gardiner, J. E.; Bull, S. D.; He, X.; James, T. D. Long-wavelength fluorescent boronate probes for the detection and intracellular imaging of peroxynitrite. *Chem. Commun.* **2017**, *53*, 12822-12825.

(37) Zhang, H.; Liu, J.; Wang, L.; Sun, M.; Yan, X.; Wang, J.; Guo, J.; Guo, W. Amino-Si-rhodamines: A new class of two-photon fluorescent dyes with intrinsic targeting ability for lysosomes. *Biomaterials*. **2018**, *158*, 10-22.

(38) Zhu, B.; Zhang, M.; Wu, L.; Zhao, Z.; Liu, C.; Wang, Z.; Duan, Q.; Wang, Y.; Jia, P. A highly specific far-red fluorescent probe for imaging endogenous peroxynitrite in the mitochondria of living cells. *Sens. Actuators, B* **2018**, *257*, 436-441.

(39) Li, D.; Cheng, J.; Wang, C.; Hu, H.; Han, F.; Li, X. Bis-reaction-trigger as a strategy to improve the selectivity of fluorescent probes. *Chem. Commun.* **2018**, *54*, 8170-8173.

(40) Zhang, J.; Zhen, X.; Zeng, J.; Pu, K. A Dual-Modal Molecular Probe for Near-Infrared Fluorescence and Photoacoustic Imaging of Peroxynitrite. *Anal. Chem.* **2018**, *90*, 9301-9307.

(41) Li, Y.; Xie, X.; Yang, X.; Li, M.; Jiao, X.; Sun, Y.; Wang, X.; Tang, B. Two-photon fluorescent probe for revealing druginduced hepatotoxicity via mapping fluctuation of peroxynitrite. *Chem. Sci*. **2017**, *8*, 4006-4011.

(42) Li, J.; Lim, C. S.; Kim, G.; Kim, H. M.; Yoon, J. Highly Selective and Sensitive Two-Photon Fluorescence Probe for Endogenous Peroxynitrite Detection and Its Applications in Living Cells and Tissues. *Anal. Chem.* **2017**, *89*, 8496-8500.

(43) Zhu, B.; Wang, Z.; Zhao, Z.; Shu, W.; Zhang, M.; Wu, L.; Liu, C.; Duan, Q.; Jia, P. A simple highly selective and sensitive hydroquinone-basedtwo-photon fluorescent probe for imaging peroxynitrite in live cells. *Sens. Actuators, B* **2018**, *262*, 380-385.

(44) Xie, X.; Tang, F.; Liu, G.; Li, Y.; Su, X. Jiao, X.; Wang, X.; Tang, B. Mitochondrial Peroxynitrite Mediation of Anthracycline-Induced Cardiotoxicity as Visualized by a Two-Photon Near-Infrared Fluorescent Probe. *Anal. Chem*. **2018**, *90*, 11629-116357.

(45) Fan, J.; Hu, M.; Zhao, P.; Peng, X. Energy transfer cassettes based on organic fluorophores: construction and applications in ratiometric sensing. *Chem. Soc. Rev*. **2013**, *42*, 29-43.

(46) Wan, Q.; Chen, S.; Shi, W.; Li, L.; Ma, H. Lysosomal pH Rise during Heat Shock Monitored by a Lysosome-Targeting Near-Infrared Ratiometric Fluorescent Probe. *Angew. Chem. Int. Ed.* **2014**, *53*, 10916-10920.

(47) Song, C.; Ye, Z.; Wang, G.; Yuan, J.; Guan, Y. A Lanthanide-Complex-Based Ratiometric Luminescent Probe Specific for Peroxynitrite. *Chem. – Eur. J.* **2010**, *16*, 6464-6472.

(48) Zhou, X.; Kwon, Y.; Kim, G.; Ryu, J.; Yoon, J. A ratiometric fluorescent probe based on a coumarin–hemicyanine scaffold for sensitive and selective detection of endogenous peroxynitrite. *Biosens. Bioelectron*. **2015**, *64*, 285-291.

(49) Jia, X.; Chen, Q.; Yang, Y.; Tang, Y.; Wang, R.; Xu, Y.; Zhu, W.; Qian, X. FRET-Based Mito-Specific Fluorescent Probe for Ratiometric Detection and Imaging of Endogenous Peroxynitrite: Dyad of Cy3 and Cy5. *J. Am. Chem. Soc*. **2016**, *138*, 10778-10781.

(50) Zhu, B.; Wu, L.; Wang, Y.; Zhang, M.; Zhao, Z.; Liu, C.; Wang, Z.; Duan, Q.; Jia, P. A highly selective and ultrasensitive ratiometric far-red fluorescentprobe for imaging endogenous peroxynitrite in living cells. *Sens. Actuators, B* **2018**, *259*, 797-802.

(51) Sun, W.; Shi, Y.; Ding, A.; Tan, Z.; Chen, H.; Liu, R.; Wang, R.; Lu, Z. Imaging viscosity and peroxynitrite by a mitochondria-targeting two-photon ratiometric fluorescent probe *Sens. Actuators, B* **2018**, *276*, 238-246.

(52) Wu, L.; Wang, Y.; Weber, M.; Liu, L.; Sedgwick, A.C.; Bull, S. D.; Huang, C.; James, T. D. ESIPT-based ratiometric fluorescence probe for the intracellular imaging of peroxynitrite. *Chem. Commun*. **2018**, *54*, 9953-9956.

(53) Zhou, D.; Li, Y.; Jiang, W.; Tian, Y.; Fei, J.; Li, C. A ratiometric fluorescent probe for peroxynitrite prepared by de novo synthesis and its application in assessing the mitochondrial oxidative stress status in cells and in vivo. *Chem. Commun.* **2018**, *54*, 11590-11593.

(54) Zhang, W.; Liu, Y.; Gao, Q.; Liu, C.; Song, B.; Zhang, R.; Yuan, J. A ruthenium(II) complex–cyanine energy transfer scaffold based luminescence probe for ratiometric detection and imaging of mitochondrial peroxynitrite. *Chem. Commun.* **2018**, *54*, 13698-13701.

(55) Cheng, D.; Pan, Y.; Wang, L.; Zeng, Z.; Yuan, L.; Zhang, X.; Chang, Y. Selective Visualization of the Endogenous Peroxynitrite in an Inflamed Mouse Model by a Mitochondria-Targetable Two-Photon Ratiometric Fluorescent Probe. *J. Am. Chem. Soc.* **2016**, *139*, 285-292.

(56) Deng, G.; Li, S.; Sun, Z.; Li, W.; Zhou, L.; Zhang, J.; Gong, P.; Cai, L. Near-infrared fluorescence imaging in the largely unexplored window of 900–1,000 nm. *Theranostics*. **2018**, *8*, 4116-4128.

(57) Cano Abad, M. F.; Benedetto, G. D.; Magalhães, P. J.; Filippin, L.; Pozzan, T. Mitochondrial pH Monitored by a New Engineered Green Fluorescent Protein Mutant. *J. Biol. Chem*. **2004**, *279*, 11521-11529.

TOC